Chemical Vapor Deposition of Hexagonal Gallium Selenide and Telluride Films from Cubane Precursors: Understanding the Envelope of Molecular Control

Edward G. Gillan[1a,b] and Andrew R. Barron*,[1a,c]

Department of Chemistry and Department of Mechanical Engineering and Materials Science, Rice University, Houston, Texas 77005

Received May 28, 1997. Revised Manuscript Received August 26, 1997[⊗]

Gallium selenide (GaSe) thin films have been grown at 325−370 °C by atmospheric pressure metal−organic chemical vapor deposition (AP-MOCVD) using the single-source precursors $[(R)Ga(\mu_3\text{-}Se)]_4$ (R = CMe_3, $CEtMe_2$, and CEt_2Me). In contrast, the growth of gallium telluride from $[(R)Ga(\mu_3\text{-}Te)]_4$ is accomplished at 285−310 °C by low-pressure metal−organic chemical vapor deposition (LP-MOCVD). Characterization of the films by Auger electron spectroscopy (AES), Rutherford backscattering (RBS), and wavelength-dispersive spectroscopy (WDS) microprobe analysis shows all the films to have Ga:E (E = Se, Te) compositions of 1:1 with a low degree of impurities (C < 2%; O < 0.1%). From X-ray diffraction (XRD) and transmission electron microscopy (TEM) the GaSe and GaTe films were found to be polycrystalline hexagonal layered GaE structures, with a preferred *c*-axis orientation independent of substrate. For GaSe this represents the thermodynamically stable phase, while hexagonal GaTe is a metastable phase that converts to the thermodynamic monoclinic form on annealing at 500 °C. Diffraction results yield appropriate lattice parameters of $a = 4.1$ Å (TEM) and $c = 16.38$ Å (XRD) for hexagonal GaTe. Crystallite and particle size measurements reveal that the as-deposited films consist of oriented ca. 10 nm crystalline particles. The formation of these hexagonal layered structures is proposed to occur as a consequence of the fragmentation of the cubane's Ga_4E_4 core during deposition, and the formation of trimeric "Ga_3E_3" building blocks.

Introduction

There has been a movement in materials chemistry toward the creation of designed materials. This suggests that the structural, physical, electronic, or magnetic properties may be controlled through the method of synthesis. In regard to thin-film growth by metal organic chemical vapor deposition (MOCVD) molecular control is defined as the ability of a precursor molecule to determine the structure (and hence some combination of properties) of a solid-state material grown from that precursor. The most intriguing advantage that MOCVD has over other film growth methods is that MOCVD processes operate far from equilibrium conditions so that kinetically rather than thermodynamically favored products may be produced. However, an important question arises: *Can the molecular structure of the precursor control the phase structure of a solid product?* While several groups have shown that thermodynamically stable phases can be prepared by MOCVD from molecules designed to represent the smallest fragment of the solid-state structure,[2,3] it is only recently that workers have demonstrated that new or metastable phases may be prepared by MOCVD or pyrolysis processes from a single molecular precursor. Notable cases where high temperature or metastable phases are formed during deposition include: cubic-GaN,[4] cubic-TaN,[5] cubic-In_2Se_3,[6] würtzite-ZnS,[7] and Zr_3N_4.[8]

Our contribution to this area has involved the use of a variety of gallium and indium sulfide precursors in the growth of GaS and InS films by MOCVD.[9] We have demonstrated that in the case of GaS the structure of the deposited film is determined by the structure of the Ga_nS_n core in the precursor molecule.[10] For example, use of the cubane precursor molecules, $[(R)Ga(\mu_3\text{-}S)]_4$, results in the growth of a new cubic phase of GaS.[11] We have clearly shown that the formation of this phase is

* To whom correspondence should be addressed (arb@ruf.rice.edu).
⊗ Abstract published in *Advance ACS Abstracts,* October 15, 1997.
(1) (a) Department of Chemistry, Rice University. (b) Present address: Department of Chemistry, University of Iowa, Iowa City, IA 52242. (b) Department of Mechanical Engineering and Materials Science, Rice University.
(2) *CVD of Compound Semiconductors*; Jones, A. C., O'Brien, P., Eds.; VCH: New York, 1996.
(3) *CVD of Nonmetals*; Rees Jr., W. E., Ed.; VCH: New York, 1996.
(4) (a) Hwang, J.-W.; Campbell, J. P.; Kozubowski, J.; Hanson, S. A.; Evans, J. F.; Gladfelter, W. L. *Chem. Mater.* **1995**, *7*, 517. (b) Hwang, J.-W.; Hanson, S. A.; Britton, D.; Evans, J. F.; Jensen, K. F.; Gladfelter, W. L. *Chem. Mater.* **1990**, *7*, 517.
(5) (a) Holl, M. M. B.; Wolczanski, P. T.; Proserpio, D.; Bielecki, A.; Zax, D. B. *Chem. Mater.* **1996**, *8*, 2468. (b) Banaszak Holl, M. M.; Wolczanski, P. T.; VanDuyne, G. D. *J. Am. Chem. Soc.* **1990**, *112*, 7989.
(6) (a) Gysling, H. J.; Wernberg, A. A.; Blanton, T. N. *Chem. Mater.* **1992**, *4*, 900. (b) Cheon, J.; Arnold, J.; Yu, K.-M.; Bourret, E. D. *Chem. Mater.* **1995**, *7*, 2273.
(7) (a) Zeng, D.; Hampden-Smith, M. J.; Duesler, E. N. *Inorg. Chem.* **1994**, *33*, 5376. (b) Nyman, M.; Pennino, S.; Hampden-Smith, M. J.; Zeng, D.; Kodas, T. T. *MRS Fall Meeting Abstract Book*; Materials Research Society: Boston, MA, 1994; p 179.
(8) Fix, R.; Gordon, R. G.; Hoffman, D. M. *Chem. Mater.* **1993**, *5*, 614.
(9) For a review see: Barron, A. R. *Adv. Mater. Opt. Electron.* **1995**, *5*, 245.
(10) MacInnes, A. N.; Power, M. B.; Barron, A. R. *Chem. Mater.* **1993**, *5*, 1344.
(11) MacInnes, A. N.; Power, M. B.; Barron, A. R. *Chem Mater.* **1992**, *4*, 11.
(12) Cleaver, W. M.; Späth, M.; Hoyk, D.; McMurdo, G.; Power, M. B.; Stuke, M.; Rankin, D. W. H.; Barron, A. R. *Organometallics* **1995**, *14*, 690.

S0897-4756(97)00388-8 CCC: $14.00

as a consequence of the retention of the cubane Ga_4S_4 core during the deposition and growth process.[12] In fact it should be noted that cubic GaS is prepared only from cubane molecules. Furthermore, it is important to note that the physical and electronic properties of the cubic GaS are distinct from the thermodynamic hexagonal phase.[13] The possibility is therefore open to the controlled synthesis of new solid-state materials with distinct and interesting physical and electronic properties. However, we have also noted that it is overly simplistic to assume that the *structure* of a precursor is the *only* factor in controlling the structure (phase) of a thin film. For example, the MOCVD of indium sulfide[14,15] and selenide[16] also teaches us that molecular control may not be sufficient.

Given the range of potential molecular structures available to synthetic inorganic chemists, the ability to create new or metastable phases of solid-state materials via molecular controls would seem to offer an unlimited range of potential materials. Unfortunately, we have demonstrated only "molecular control " as a principle to explain *with hindsight* the structure of deposited films and have insufficient knowledge to *predict* structure. If molecular control is to become a predictive science, we propose that an understanding of the intimate mechanism of precursor decomposition and the structural factors that allow for (or preclude) molecular control may provide sufficient information for further modifications toward the design of successful single-source precursors for new designed materials. This may be described as understanding the envelope of molecular control.

The objective of our present studies has been to continue our exploration of the chemistry of group 13 chalcogenides with particular reference to the idea that thin-film phase formation and/or morphology may be controlled by the molecular structure, core stability, and decomposition mechanism of the precursor compounds. One of our target areas is the development and understanding of molecular control during MOCVD of 13−16 materials. In this regard we have continued our investigation of the MOCVD of the group 13 chalcogenide cubane precursor compounds $[(R)Ga(\mu_3\text{-}E)]_4$ (**I**) with a detailed study of the growth of gallium selenide and telluride.

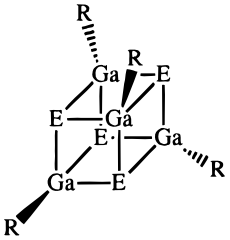

(**I**) E = S, Se, Te

In a preliminary communication,[17] we reported the MOCVD of thin films (≤300 Å) of GaSe with unusual nanoparticle morphologies using the cubane precursor $[(^tBu)Ga(\mu_3\text{-}Se)]_4$. We now describe full details of the MOCVD of GaSe and GaTe films from the cubane precursors $[(R)Ga(\mu_3\text{-}E)]_4$ [E = Se, Te, and R = CMe_3 (^{t}Bu, **II**), $CEtMe_2$ (**III**), CEt_2Me (**IV**)] and discuss the control their decomposition exerts on the structure of the resulting films.

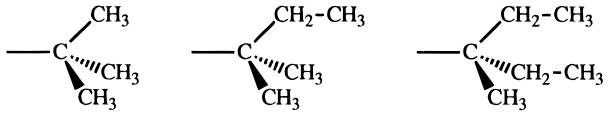

(**II**) (**III**) (**IV**)

Results and Discussion

Precursor Stability and Volatility. The syntheses and characterization of the cubane chalcogenides, $[(R)Ga(\mu_3\text{-}E)]_4$, employed in this study have been described previously.[18−20] All the compounds are molecular solids with varying degrees of thermal and oxidative stability. None of the cubane compounds are pyrophoric. The selenide cubanes are stable for months in air; however, the tellurium cubanes turn dark brown after a few minutes of exposure to atmospheric conditions. This is presumably as a consequence of the oxidation of the telluride to metallic tellurium, i.e., Te^{2-} to Te^0. Thus the tellurides should be handled and stored under a dry inert (N_2, Ar, etc.) atmosphere.

We have previously determined the volatilization−decomposition window of the cubane compounds using thermogravimetric analysis (TGA).[20] As can be seen from Table 1, sublimation[21] occurs upon heating in an inert carrier gas flow at temperatures between 200 and 300 °C. In addition, under dynamic vacuum (ca. 0.2 Torr) the volatilization temperature decreases by nearly 100 °C for each of the cubane compounds.[20] This is particularly useful for the telluride cubane compounds, $[(R)Ga(\mu_3\text{-}Te)]_4$, which undergo partial decomposition during sublimation under atmospheric pressure (see Figure 1).

MOCVD of Gallium Selenide Films. The deposition of gallium selenide films from the $[(R)Ga(\mu_3\text{-}Se)]_4$ (R = CMe_3, $CEtMe_2$, CEt_2Me) cubane precursors is readily achieved under atmospheric pressure conditions using a horizontal flow hot-wall design (see Experimental Section). The various cubane compounds were

(13) See for example: (a) MacInnes, A. N.; Power, M. B.; Barron, A. R.; Jenkins, P. P.; Hepp, A. F. *Appl. Phys. Lett.* **1993**, *62*, 711. (b) MacInnes, A. N.; Power, M. B.; Barron, A. R.; Jenkins, P. P.; Hepp, A. F. *Mater. Res. Soc., Symp. Proc.* **1993**, *282*, 111. (c) Tabib-Azar, M.; Kang, S.; MacInnes, A. N.; Power, M. B.; Jenkins, P. P.; Hepp, A. F.; Barron, A. R. *Appl. Phys. Lett.* **1993**, *63*, 625. (d) Jenkins, P. P.; MacInnes, A. N.; Tabib-Azar, M.; Barron, A. R. *Science* **1994**, *263*, 1751.

(14) MacInnes, A. N; Cleaver, W. M.; Barron, A. R.; Power, M. B.; Hepp, A. F. *Adv. Mater. Opt. Electron.* **1992**, *1*, 229.

(15) MacInnes, A. N.; Power, M. B.; Hepp, A. F.; Barron, A. R. *J. Organomet. Chem.* **1993**, *449*, 95.

(16) Stoll, S. L.; Barron, A. R., submitted for publication.

(17) Stoll, S. L.; Gillan, E. G.; Barron, A. R. *Chem. Vap. Deposition* **1996**, *2*, 182.

(18) Power, M. B.; Ziller, J. W.; Tyler, A. N.; Barron, A. R. *Organometallics* **1992**, *11*, 1055.

(19) Harlan, C. J.; Gillan, E. G.; Bott, S. G.; Barron, A. R. *Organometallics* **1996**, *15*, 5479.

(20) Gillan, E. G., Bott, S. G.; Barron, A. R. *Chem. Mater.* **1997**, *9*, 796.

(21) The uniform mass loss of $[(EtMe2C)Ga(\mu_3\text{-}Se)]_4$ under vacuum is accompanied by a broad endothermic event characteristic of sublimation. In some cubanes this thermal event is quite broad or is shifted near the end of the sublimation process, while in other cases melting occurs as evidenced by a sharp endotherm; therefore, the position of this thermal event was not a good indicator of relative cubane volatilities (sublimation temperature). To allow a direct comparison of the relative volatility of the various cubanes, a sublimation temperature was defined as the point when 20% mass loss had occurred and T_{sub} values were determined for each compound under both flowing inert gas (nitrogen or argon) and dynamic vacuum (P < 0.2 Torr) conditions.

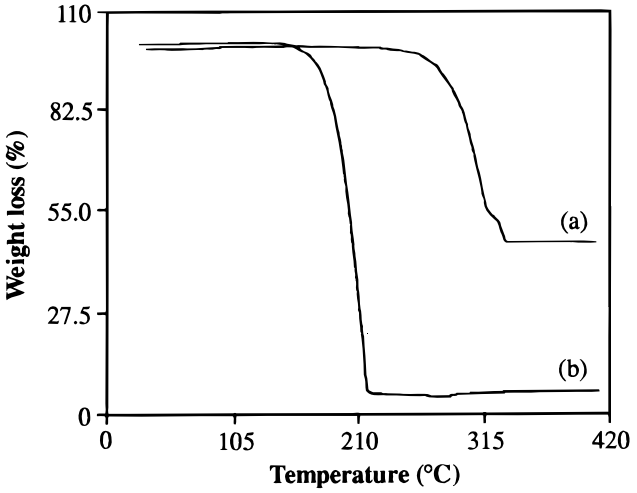

Figure 1. Thermogravimetric analysis of $[(Et_2MeC)Ga(\mu_3\text{-}Te)]_4$ at (a) atmospheric pressure and (b) under dynamic vacuum (ca. 0.2 Torr).

Table 1. Sublimation Temperatures for the Selenide and Telluride Cubane Precursor Compounds $[(R)Ga(\mu_3\text{-}E)]_4$

	T_{sub} (°C)	
precursor	760 Torr[a]	0.2 Torr[a]
$[(Me_3C)Ga(\mu_3\text{-}Se)]_4$	241	149
$[(EtMe_2C)Ga(\mu_3\text{-}Se)]_4$	245	152
$[(Et_2MeC)Ga(\mu_3\text{-}Se)]_4$	284	165
$[(Me_3C)Ga(\mu_3\text{-}Te)]_4$	273[b]	172
$[(EtMe_2C)Ga(\mu_3\text{-}Te)]_4$	275[b]	195
$[(Et_2MeC)Ga(\mu_3\text{-}Te)]_4$	288[b]	194

[a] Non-SI units: 1 Torr = 1 mmHg = 133 Pa. [b] Sublimation with decomposition.

heated to between 230 and 270 °C just prior to the entrance of the deposition furnace (see Table 2). The optimum growth temperature was determined as the point where a majority of the precursor decomposed near the center of the heated furnace. This temperature ranged between 345 and 350 °C for all three precursors (Table 2). Typically deposition rates were on the order of 20 Å min^{-1}. Pale orange films were grown on SiO_2 substrates, while reflective, mirrorlike, adherent films (Scotch tape test) grew on Si (100) and GaAs (100) wafers. A repeating spectrum of colors (yellow to green) was evident on the Si and GaAs wafers as the deposition proceeded, indicative of the changing film thickness producing interference fringes in the visible spectrum.[22]

Previous work on $[(Me_3C)Ga(\mu_3\text{-}S)]_4$ demonstrated that the cubane undergoes decomposition via successive loss of the *tert*-butyl substituents,[12] suggesting that decomposition occurs via either β-hydride elimination and/or Ga−C homolytic bond cleavage.[23] It is surprising therefore that the predominant volatile byproduct isolated from the MOCVD of $[(Me_3C)Ga(\mu_3\text{-}Se)]_4$ at 350 °C was Me_3CCMe_3 (2,2,3,3-tetramethylbutane). Minor amounts of $Me_2C{=}CH_2$ and Me_3CH were also observed (5% and 1% that of Me_3CCMe_3, respectively).[24] It is worth noting that the vapor phase (and solution) decomposition of $Ga(CMe_3)_3$ occurs via the formation of the $Me_3C^{\bullet}$ radical; however, Me_3CCMe_3 is not observed.[25] The presence of coupled alkyl ligands (i.e., Me_3CCMe_3) suggests a cubane coupling reaction in either the vapor phase or on the surface occurs during MOCVD. Such a reaction (reductive coupling) would lead to the formation of gallium−gallium bonds. This proposal is discussed in more detail below.

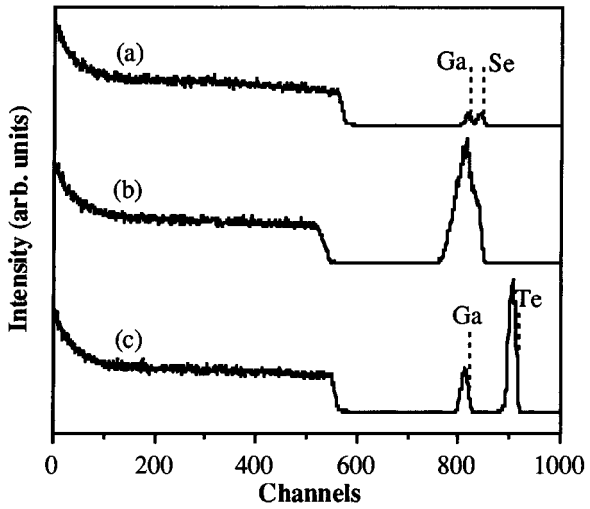

Figure 2. RBS spectra for (a) a 100 Å GaSe film grown from $[(Me_3C)Ga(\mu_3\text{-}Se)]_4$ at 335 °C, (b) a 2000 Å GaSe film grown from $[(Me_3C)Ga(\mu_3\text{-}Se)]_4$ at 350 °C, and (c) a 650 Å GaTe film grown from $[(Me_3C)Ga(\mu_3\text{-}Te)]_4$ at 285 °C.

Rutherford backscattering spectroscopy (RBS), Auger electron spectroscopy (AES), and wavelength-dispersive spectroscopy (WDS) microprobe analysis were employed for film analysis. Film thicknesses of ca. 300 Å were preferable for RBS analysis since the characteristic gallium and selenium peaks are closely spaced (Figure 2a,b). Thicker (>0.1 μm) films are preferred for AES depth profiling and microprobe analysis, since surface impurities (oxygen and adsorbed carbon) can complicate bulk analysis in both of these cases. As Table 2 shows, the overall Ga:Se ratios of films grown from each cubane are close to 50:50, indicating that the films are essentially equimolar in each element and reflective of the Ga and Se ratio in the precursor. From AES, carbon was present at levels less than 2 atomic % and oxygen was not detected (estimated <0.1%) after sputtering off the surface layer. The as-grown GaSe films are stable for long periods under ambient atmospheric conditions, as evidenced by essentially unchanged compositional results (including oxygen) on a film analyzed 1 year after growth. The elemental composition of annealed films (see below) are essentially unchanged when compared to the as-deposited ones; for example, films obtained from $[(EtMe_2C)Ga(\mu_3\text{-}Se)]_4$ have a Ga:Se of 46:54 before and 47:53 after annealing.

The crystallinity and phase of as-deposited and annealed films were examined by thin-film X-ray diffraction (XRD) on films grown to ca. 0.2−0.8 μm thicknesses. The GaSe films grown from $[(Me_3C)Ga(\mu_3\text{-}Se)]_4$ at 350 °C were crystalline with reflections consistent with the thermodynamic, layered hexagonal phase of GaSe (h-

(22) Plisken, W. A.; Conrad, E. E. *IBM J. Res. Dev.* **1964**, *8*, 43.

(23) The formation of both $Me_2C{=}CH_2$ (isobutene) and Me_3CH (isobutane) has been observed in thermal desorption experiments, Weinberg, H., personal communication. However, at present it is unclear whether the isobutene is formed by a β-hydride elimination reaction or from the degradation of isobutyl radicals formed from homolytic bond cleavage.

(24) It should be noted that Me_3CCMe_3 (bp = 107 °C) is easier to isolate than either $Me_2C{=}CH_2$ or Me_3CH, which are more volatile with boiling points of −7 and −12 °C, respectively.

(25) (a) Cleaver, W. M.; Barron, A. R.; Zhang, Y.; Stuke, M. *Appl. Surf. Sci.* **1992**, *54*, 8. (b) Zhang, Y.; Cleaver, W. M.; Stuke, M.; Barron, A. R. *Appl. Phys. A* **1992**, *55*, 261.

Table 2. Deposition Parameters and Results on GaSe Films Grown by Atmospheric Pressure MOCVD from [(R)Ga(μ_3-Se)]$_4$ Precursors

precursor	precursor temp (°C)	deposition temp (°C)	crystalline phase	analysis (Ga:Se)	crystallite size (Å)[c]
[(Me_3C)Ga(μ_3-Se)]4	230−245	350	h-GaSe	46:54[b]	135
[($EtMe_2C$)Ga(μ_3-Se)]$_4$	240−250	345	h-GaSe[a]	46:54	95[d]
[(Et_2MeC)Ga(μ_3-Se)]$_4$	260−270	350	h-GaSe[a]	44:56	100[e]

[a] Poorly crystalline film as-deposited but crystallizes on annealing at 450 °C. [b] RBS: 53:47 ratio (300 Å film); Auger: 55:45 ratio. [c] XRD measurements. [d] After annealing at 450 °C for 1.5 h. [e] After annealing at 450 °C for 3.5 h.

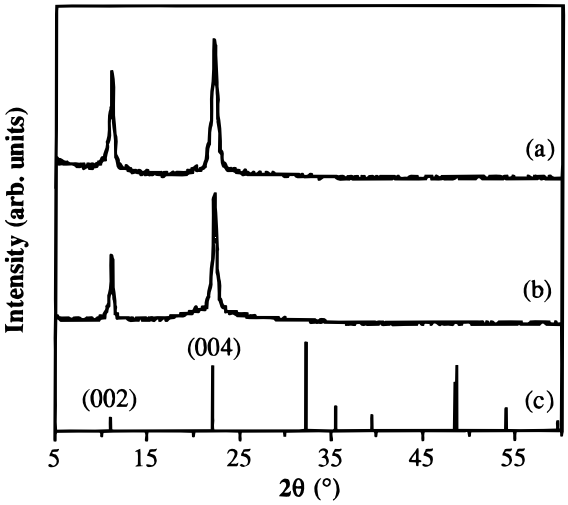

Figure 3. Thin-film X-ray diffraction results for GaSe films grown by atmospheric CVD from [(Me_3C)Ga(μ_3-Se)]$_4$ at 350 °C deposited on (a) Si (100) and (b) fused silica. The standard pattern for hexagonal GaSe (JCPDS 37,0931) is shown for comparison (c).

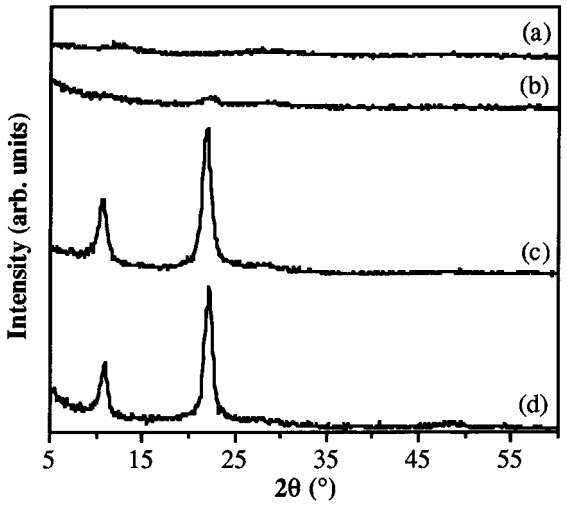

Figure 4. Thin-film X-ray diffraction results for GaSe films grown by atmospheric CVD on Si(100) from [($EtMe_2C$)Ga(μ_3-Se)]$_4$ at 345 °C (a) as-grown, (b) annealed at 400 °C for 17 h, (c) annealed at 450 °C for 1.5 h, and (d) from [(Et_2MeC)Ga(μ_3-Se)]$_4$ at 350 °C and then annealed at 450 °C for 3.5 h.

GaSe); see Figure 3. Use of either [($EtMe_2C$)Ga(μ_3-Se)]$_4$ or [(Et_2MeC)Ga(μ_3-Se)]$_4$ as the precursor resulted in the growth of poorly crystalline h-GaSe (broad, low-intensity peaks). However, these films achieve comparable crystallinity to those grown from [(Me_3C)Ga(μ_3-Se)]$_4$ upon annealing at 450 °C (see Figure 4).

As can be seen from Figures 3 and 4, the (00*l*) peaks are predominant in the XRD for all GaSe films, including films grown on fused quartz. Thus, the films have an apparent preferred *c*-axis orientation nearly perpendicular to the plane of the substrate. Rocking curve

Table 3. Measured *d* Spacing (Å) for h-GaE Films Grown from [(Me_3C)Ga(μ_3-E)]$_4$ (E = Se, Te)

	d spacing (Å)	
hkl	h-GaSea	h-GaTe
002[b]	7.97 (7.998)	8.18
004[b]	3.99 (3.999)	4.09
101	3.13 (3.183)	3.57
104	2.50 (2.521)	
106	2.03 (2.061)	2.13
107	1.88 (1.869)	
200	1.63 (1.624)	
1011	1.34 (1.327)	
1012	1.23 (1.233)	1.23
300	1.09 (1.083)	
1015	1.03 (1.013)	1.06

[a] Literature values for h-GaSe (JCPDS 37,0931) are given in parentheses. [b] Measured from XRD. All other data obtained from electron diffraction.

X-ray analysis showed that these oriented films are polycrystalline, not single crystal. The calculated lattice parameter for the as-deposited h-GaSe films (c = 15.95 Å) is close to the literature value (a = 3.75 Å, c = 15.995 Å).[26] The broadening associated with the XRD peaks can be correlated with the size of crystalline domains in the film using the Scherrer equation.[27] The average crystallite sizes derived from the (004) reflections are tabulated in Table 2. Note that these values are strictly related to crystallinity along the *c*-axis and roughly equate to 15 double Se−Ga−Ga−Se layers each being 8 Å high (see below). Table 3 summarizes the diffraction results for the h-GaSe films grown from [(Me_3C)-Ga(μ_3-Se)]$_4$ at 350 °C.

Our previous results on very thin (ca. 300 Å) GaSe films analyzed by transmission electron microscopy (TEM) show that nearly spherical nanoparticles (44 nm on average) join into snakelike chains on the substrate surface during the initial stages of the deposition.[17] A cross-sectional TEM bright-field (BF) image of a 0.8 μm thick GaSe film grown on Si from [(Me_3C)Ga(μ_3-Se)]$_4$ at 350 °C (Figure 5a) demonstrates that this "nanoparticle" motif continues throughout the film growth process (Figure 5b). The particle sizes average nearly 100 Å, which is consistent with the calculated crystallite sizes from thin-film XRD (Table 2). The electron diffraction pattern from a few of these crystallites demonstrates that they are well crystallized, since a partial spot pattern is evident (Figure 5c). The ring pattern closely agrees with h-GaSe yielding a = 3.7 Å and c = 16.1 Å. The rings show a preference for (10*l*) reflections consistent with the orientational effects observed by XRD (see above). A corresponding dark-field image using the most intense diffraction ring shows

(26) *Pearson's Handbook of Crystallographic Data for Intermetallic Phases*, 2nd ed.; Villars, P.; Calvert, L. D., Eds.; ASM Intl.: Materials Park, OH, 1991.
(27) Warren, B. E. *X-ray Diffraction*; Dover Publications Inc.: New York, 1990; p 253.

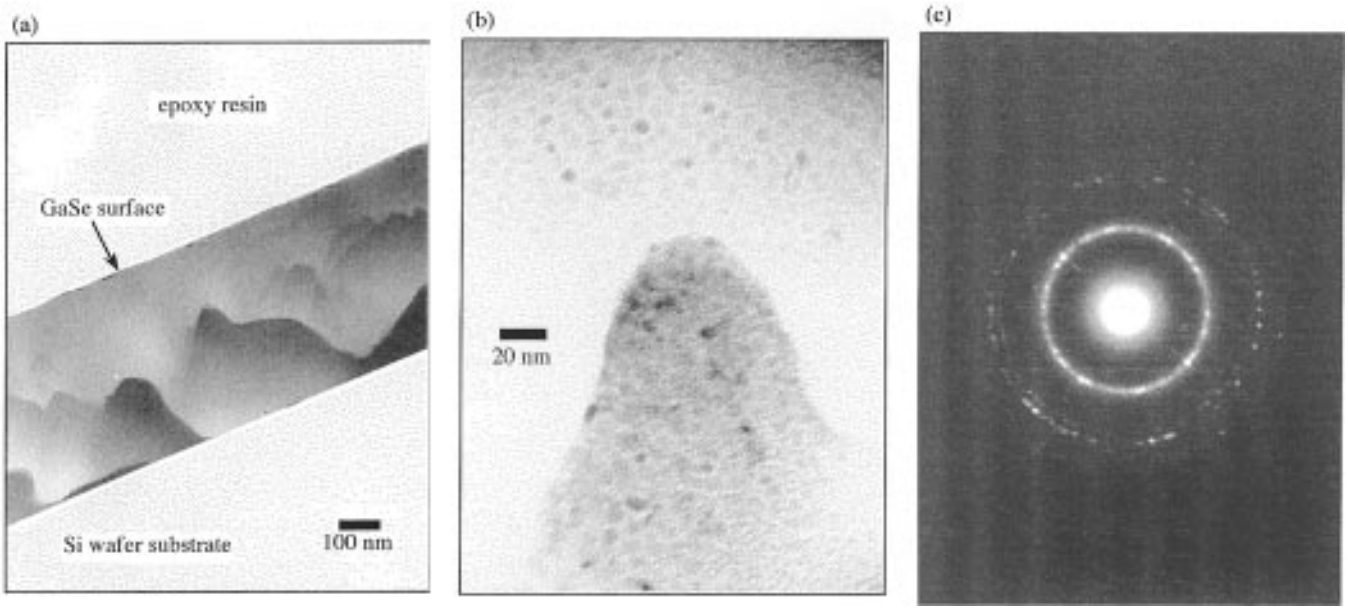

Figure 5. TEM results on GaSe films grown on Si from $[(Me_3C)Ga(\mu_3\text{-}Se)]_4$ at 350 °C. Shown are (a) the film cross section, (b) a high-resolution bright-field image, and (c) an electron diffraction pattern.

that most of the spherical particles imaged in BF diffract and contribute to this diffraction. The regions between the particles do not diffract well and may consist of misoriented or disordered regions. It is common in depositions of layered materials (e.g., BN and graphite) to see van der Waals orientation along the *c*-axis but misorientation of grains along the *ab* plane (turbostratic).[28] Table 3 summarizes the electron diffraction results for the h-GaSe films grown from $[(Me_3C)Ga(\mu_3\text{-}Se)]_4$ at 350 °C.

The surface morphology of these thick films deposited in this study appear to be a natural extension of the TEM results. The surface of the GaSe films appear textured which when viewed at higher magnification shows the distinctive particle-like morphology (Figure 6a,b), with a feature size of ca. 0.2 μm. The particle-like morphology in the GaSe films suggests the occurrence of some gas-phase decomposition above the substrate surface. This may be concurrent with surface-initiated growth that "knits" together these particles into a cohesive film consisting of larger particle domains. The surface and cross-sectional morphologies indicates that these films are dense and free of large voids or defects (Figure 6c).

Crystalline GaSe films deposited from $[(Me_3C)Ga(\mu_3\text{-}Se)]_4$ at 350 °C were annealed at 500 °C for 36 h and showed essentially no increase in *c*-axis registry (i.e., the calculated crystallite size was unchanged). In contrast, preliminary results on GaSe films grown at 350 °C using a heated substrate "warm-walled" chamber (see Experimental Section) demonstrate that if cubane decomposition can be induced to occur primarily on the substrate surface, highly *c*-axis oriented hexagonal films may be obtained (Figure 7). From XRD measurements these films have a crystallite size (along the *c*-axis) of 360 Å, equivalent to 45 Se−Ga−Ga−Se layers. Further studies with this warm-wall geometry are in progress.

The stoichiometric h-GaSe phase is reported to be a moderate bandgap semiconductor with E_g values of 2.0 eV.[29] Films of h-GaSe grown on SiO_2 substrates from cubane precursors show absorption cutoffs of 2.4 eV, consistent with the literature values (Figure 8a). The interference fringes prior to absorption may in general be used to calculate the refractive index of the film if an accurate film thickness is known.

Temperature-Dependent Growth of GaSe. The growth of GaSe films at temperatures above and below the optimum growth temperature (ca. 350 °C) were explored with the *tert*-butyl precursor, $[(Me_3C)Ga(\mu_3\text{-}Se)]_4$. Table 4 lists deposition conditions and selected results.

At 325 °C the majority of the precursor sublimes intact through the heated deposition zone; however, the slow growth of an amorphous GaSe film also occurs. Once deposited, the amorphous GaSe films, having a composition near 50:50 (Ga:Se), do not crystallize to h-GaSe until annealing at 450 °C for 1 h. In various depositions at low temperatures (325−335 °C) there is evidence of a highly oriented component to the GaSe films. A sharp peak with a *d* spacing of 2.0 Å ($2\theta \approx 45°$), corresponding to ca. 900 Å crystallite size (Figure 9), was observed which had a high degree of orientational order as determined by rocking curve analysis. The position of this peak was independent of the growth surface (Si, GaAs, or SiO_2); see Figure 9a,b. It remains present even as hexagonal GaSe crystallizes on annealing films on GaAs (Figure 9d) but is absent from films crystallized on Si at 450 °C. In analogy with previous work on GaS, this oriented peak could correspond to the (220) reflection of a cubic phase which would yield a lattice constant of 5.66 Å, close to what would be expected for cubic-GaSe, e.g., the gallium deficient cubic Ga_2Se_3 phase has $a = 5.43$ Å (JCPDS 5,0724). More structural work will be necessary to definitively determine the origin of this highly oriented component.

Deposition at 340 °C is where poorly crystalline h-GaSe is first evident by thin-film XRD (Figure 10a). Increasing deposition temperature results in films of

(28) (a) *Handbook of Carbon, Graphite, Diamond and Fullerene*; Pierson, H. O.; Noyes: Park Ridge, NJ, 1993. (b) Zheng, T.; Reimers, J. N.; Dahn, J. R. *Phys. Rev. B* **1995**, *51*, 734.

(29) *Data in Science and Technology: Semiconductors*; Madelung, O., Ed.; Springer-Verlag: New York, 1992.

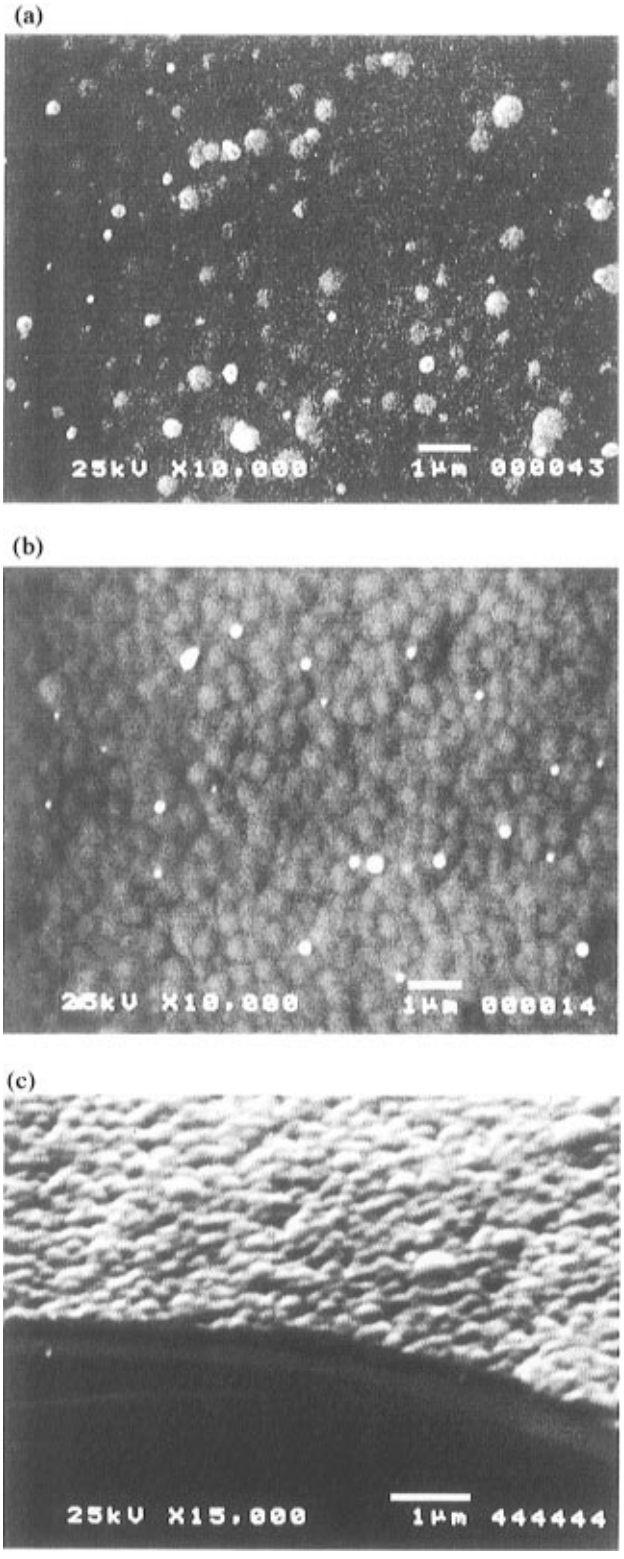

Figure 6. Scanning electron micrographs of deposited GaSe films grown on Si from (a) $[(Me_3C)Ga(\mu_3\text{-}Se)]_4$ at 350 °C and (b and c) $[(EtMe_2C)Ga(\mu_3\text{-}Se)]_4$ at 345 °C.

increased crystallinity (Figure 10b). However, at 370 °C a significant portion of the precursor decomposes prior to the center of the furnace, although fringes of the deposition also reach to the center zone where the substrates are located. The deposited phase is crystalline, and the peaks may be indexed as h-GaSe though (*hkl*), (*hk*0), and (*h*0*l*) peaks are also prominent in addition to (00*l*) lines, suggesting a more random orientation of the crystalline domains (Figure 10c). It

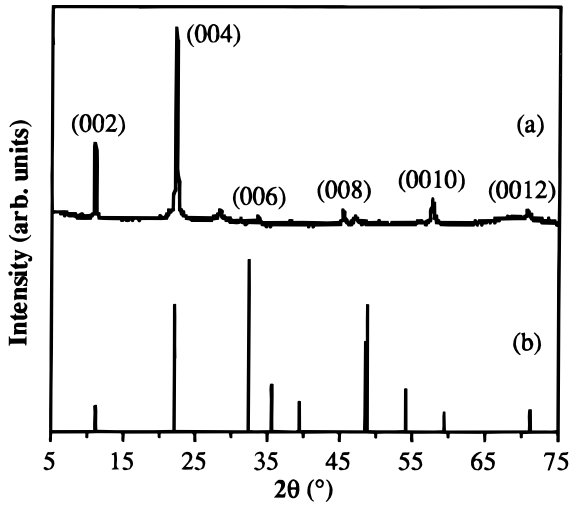

Figure 7. Thin-film XRD of (a) an h-GaSe film grown on Si (100) from $[(Me_3C)Ga(\mu_3\text{-}Se)]_4$ at ca. 350 °C using a warm-walled (250 °C) MOCVD chamber; and (b) the standard pattern for hexagonal GaSe (JPDS 37,0931).

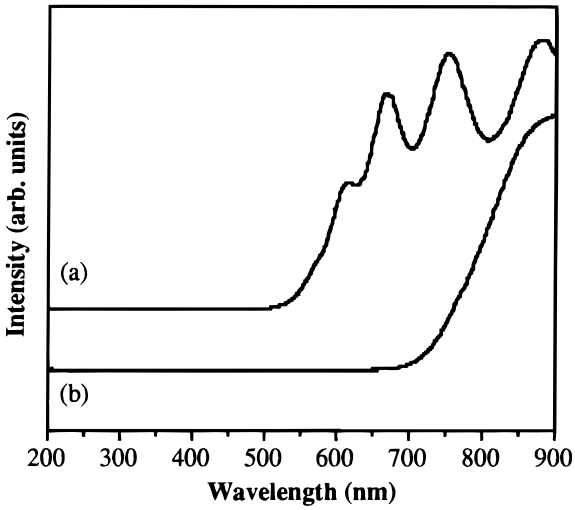

Figure 8. Transmission UV−vis spectra for (a) an h-GaSe film grown at 350 °C from $[(Me_3C)Ga(\mu_3\text{-}Se)]_4$ and (b) an h-GaTe film grown at 310 °C from $[(EtMe_2C)Ga(\mu_3\text{-}Te)]_4$. Spectra are offset on the *y*-axis for clarity.

Table 4. Temperature Dependence of the MOCVD Growth of GaSe Thin Films from $[(Me_3C)Ga(\mu_3\text{-}Se)]_4$

deposition temp (°C)	crystalline phase	analysis (Ga:Se)	crystallite size (Å)[b]	optical bandgap (eV)
325	amorphous[a]	51:49	n/a	2.40
340	poorly crystalline h-GaSe	50:50	≤60	2.35
350	h-GaSe (c = 15.95 Å)	46:54	130	2.35
370	h-GaSe (c = 32 Å)	48:52	220	2.20

[a] Also contains highly oriented possibly cubic phase; see text. [b] From XRD measurements.

is interesting to note that the presence of a strong reflection for (0 0 10) at 28° is consistent with h-GaSe with a doubled *c*-axis (JCPDS 29,0628: a = 3.775 Å, c = 31.99 Å). The *c*-axis relationship between these two modifications is shown in Figure 11.

As Table 4 shows, the crystallinity of the deposited phase generally increases as the deposition temperature increases. The deposition rate also increases significantly, and this may give rise to the *c*-axis doubled disordered structure. Even though the crystalline structure/stacking of the GaSe layers changes, the

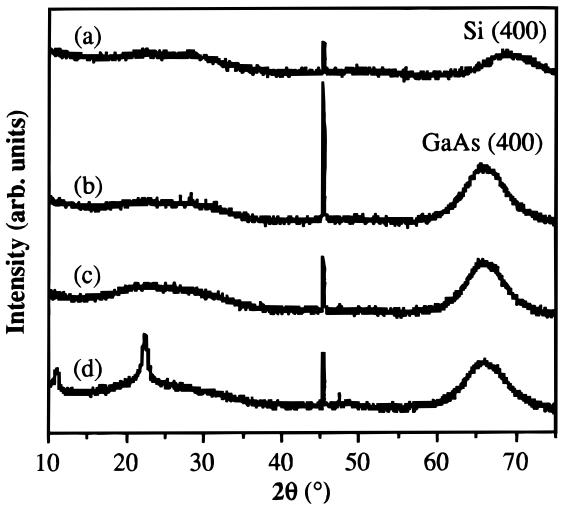

Figure 9. Thin-film XRD of oriented phase present in GaSe films grown from $[(Me_3C)Ga(\mu_3\text{-}Se)]_4$ at 325 °C (a) grown on Si then annealed at 400 °C, (b) as grown on GaAs, (c) film from (b) annealed at 400 °C, and (d) film in (c) further annealed to 450 °C. In all scans, the films were oriented to obtain a maximum intensity of the peak at 45°.

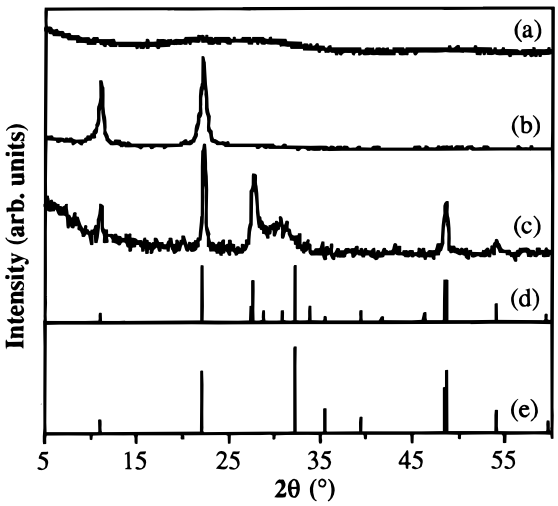

Figure 10. Thin-film X-ray diffraction results for GaSe films grown by atmospheric CVD from $[(Me_3C)Ga(\mu_3\text{-}Se)]_4$ on Si at (a) 340, (b) 350, and (c) 370 °C. The standard pattern for h-GaSe with a doubled *c*-axis (32 Å, JCPDS 29,0628) and the thermodynamic h-GaSe (JCPDS 37,0931) are shown for comparison (d and e, respectively).

composition is constant and the optical gap does not change significantly.

MOCVD of Gallium Telluride Films. To enable volatilization under atmospheric pressure conditions, the gallium telluride cubane compounds, $[(R)Ga(\mu_3\text{-}Te)]_4$ (R = CMe_3, $CEtMe_2$, CEt_2Me), require heating to temperatures approaching that of their decomposition (see above).[20] In contrast, the gallium telluride cubane compounds are volatilized between 150 and 190 °C under reduced pressure (0.01−0.3 Torr), well below their decomposition temperatures. The growth of gallium telluride thin films from $[(R)Ga(\mu_3\text{-}Te)]_4$ was therefore performed under low-pressure MOCVD conditions in order to minimize precursor decomposition during the volatilization and transport process.

Visibly smooth, reflective gallium telluride films were grown on Si (100) and GaAs (100) at 285−310 °C (Table 5). The deposition temperatures required for the telluride film growth are nearly 50 °C lower than those necessary for GaSe (see Table 2). As with the GaSe films, the GaTe films adhered well (Scotch tape test) to the substrates. Films grown on fused quartz glass for optical measurements were dark orange in color.

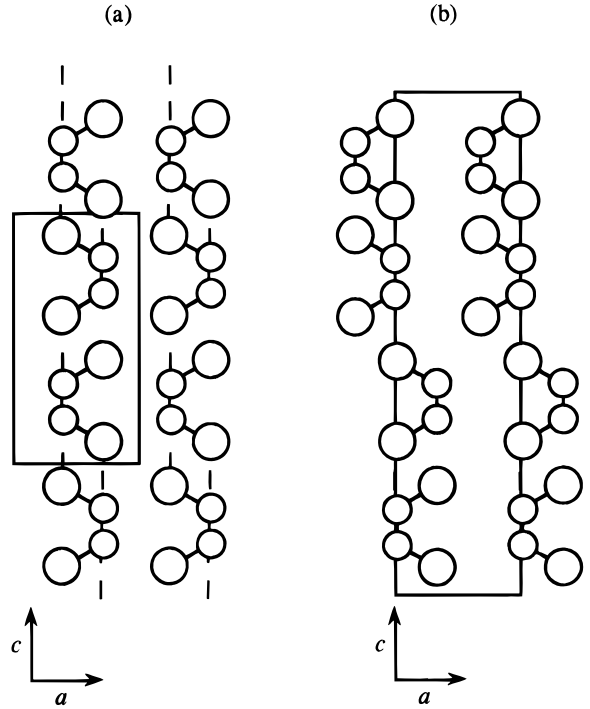

Figure 11. Structural relationship of (a) "normal" h-GaSe and (b) doubled *c*-axis h-GaSe. Note, Ga atoms are shown as the small circles and unit cell and crystal axis are given for clarity.

Elemental analyses of the GaTe films from the various cubane precursors yielded results indicating equimolar compositions, i.e., the Ga:Te ratio is nearly 50:50 in all the films (Table 5). Carbon levels were below the AES detection limit (estimated < 0.1%) and microprobe analyses indicated the presence of less than 3 atomic % oxygen, which includes any surface adsorbed species. As may be expected, the GaTe films are more air sensitive than their GaS and GaSe counterparts. Significant surface oxidation/hydrolysis occurs after standing for a few weeks in air. AES analysis indicated that films analyzed one week after deposition contained 5−10 atomic % oxygen. RBS data confirm the Ga:Te ratio to be 50:50; see Figure 2c.

The GaTe film morphology is similar to that of GaSe discussed above, except the feature size is smaller, on the order of 0.1 μm, possibly as a consequence of the lower deposition temperature (Figure 12). It is interesting to note that the feature size observed for the GaTe films grown from $[(EtMe_2C)Ga(\mu_3\text{-}Te)]_4$ at 310 °C are comparable to those in the GaSe films grown at 350 °C. However, the GaTe films grown from $[(Me_3C)Ga(\mu_3\text{-}Te)]_4$ and $[(EtMe_2C)Ga(\mu_3\text{-}Te)]_4$ at 285 °C have significantly smaller features. This observation suggests a temperature dependence for the "particle" growth.

The XRD data on the low-pressure MOCVD GaTe films show a preferred orientation (*c*-axis) hexagonal phase (h-GaTe) analogous to that found for GaSe, irrespective of the precursor (Figure 13). The *c*-axis unit-cell dimensions (c = 16.38 Å) are slightly larger than h-GaSe (c = 15.95 Å as grown, c = 15.995 Å literature[26]) as expected from the larger chalcogenide

Table 5. Deposition Parameters and Results of Low-Pressure MOCVD of GaTe Films Grown from [(R)Ga(μ_3-Te)]$_4$

precursor	precursor temp (°C)	deposition temp (°C)	pressure (Torr)	crystalline phase	analysis (Ga:Te)	crystallite size (Å)[a]
[(Me_3C)Ga(μ_3-Te)]$_4$	150−160	285	10^{-3}	h-GaTe	48:52	110
[($EtMe_2C$)Ga(μ_3-Te)]$_4$	160−170	310	0.3	h-GaTe	48:52	125
[(Et_2MeC)Ga(μ_3-Te)]$_4$	180−190	285	0.3	h-GaTe	46:54	115

[a] XRD measurements.

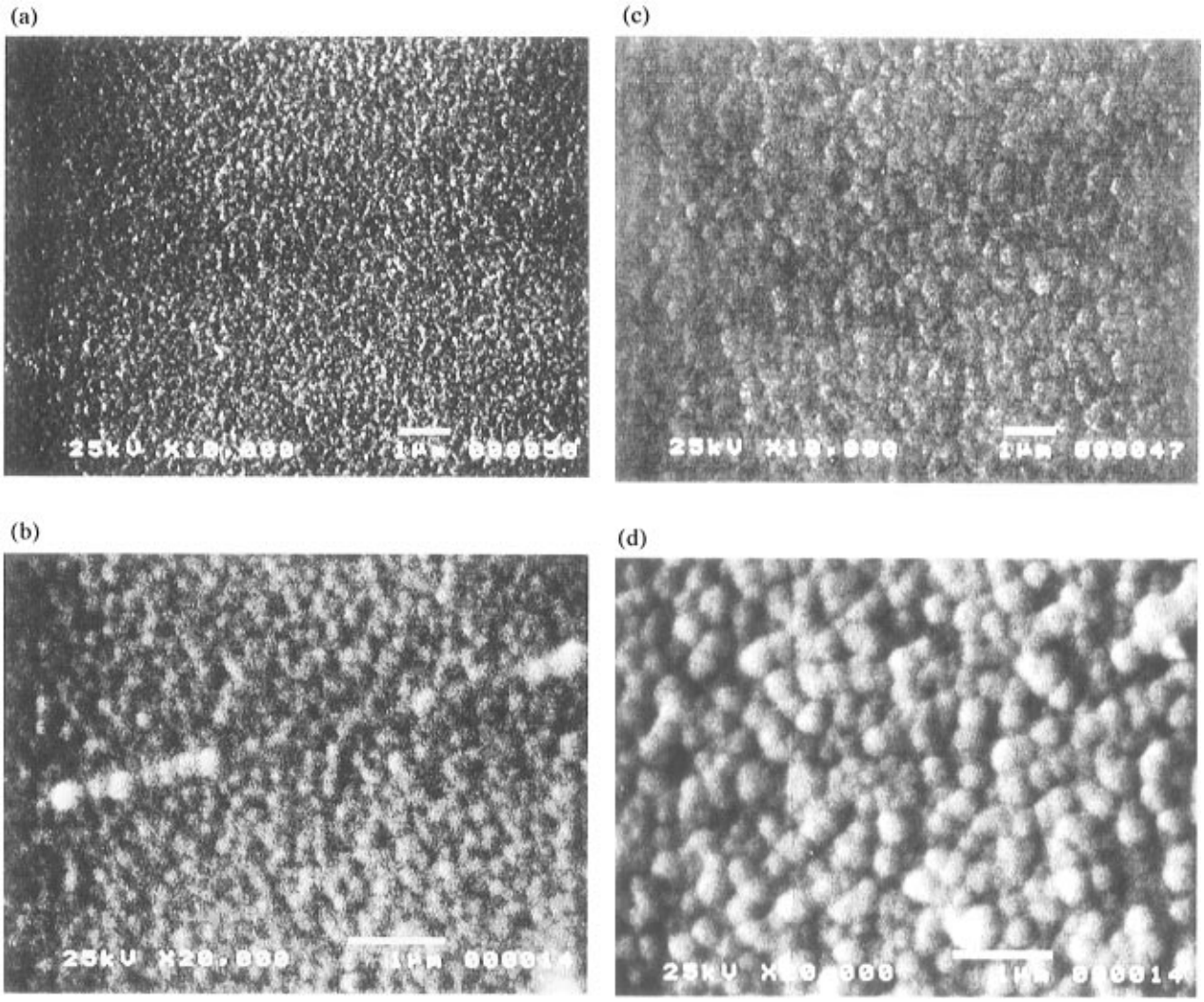

Figure 12. Scanning electron micrographs of deposited GaTe film films grown on Si from (a and b) [(Me_3C)Ga(μ_3-Te)]$_4$ at 285 °C, and (c and d) [($EtMe_2C$)Ga(μ_3-Te)]$_4$ at 310 °C.

(covalent radii: Se = 1.17 Å versus Te = 1.37 Å). The *c*-axis oriented h-GaTe films have a crystallite sizes (Table 5) similar to those observed for the h-GaSe discussed above.

From a study of the thermodynamic binary Ga/Te phase diagram,[30] the stable phase with a Ga:Te composition of 1:1 has a monoclinic structure (m-GaTe, JCPDS 33-0571, $a = 17.404$, $b = 4.077$, $c = 10.456$ Å, $\beta = 104.44°$). The only previous report of a hexagonal phase of GaTe (GaS type; $a = 4.06$, $c = 16.96$ Å) was by Semiletov and Vlasov,[31] who identified this phase by electron diffraction measurements of very thin films (ca. 300 Å) deposited by physical methods onto substrates at room temperature. In addition, they reported that the h-GaTe is a metastable phase and converts to the thermodynamic monoclinic phase upon heating; however, they found that the monoclinic phase formed directly when the substrate (NaCl) was heated to 200 °C. In a similar manner, our MOCVD grown h-GaTe films are converted to m-GaTe after annealing at 500 °C for 10 h (Figure 13c).

One important feature of the annealing of h-GaTe to m-GaTe is that the film's preferred orientation is retained. The *c*-axis ordering of h-GaTe requires the GaTe sheets being parallel to the growth surface. On conversion to m-GaTe the sheets are still parallel to the substrate except now the lattice parameters have changed and some geometric features of the layers are different. Structural models for h-GaSe and m-GaTe drawn from crystallographic data are shown in Figure 14. The unit cells are outlined for clarity. While the (00*l*) reflections are observed in the as deposited h-GaTe, the annealed m-GaTe films only exhibit reflections from the [−201] direction, suggesting that the localized twist

(30) *Binary Alloy Phase Diagrams*, 2nd ed.; Massalski, T. B., Ed.; ASM International: Materials Park, OH, 1990; Vol. 2, pp 1864−1865.
(31) Semiletov, S. A.; Vlasov, V. A. *Sov. Phys.-Crystallogr.* **1964**, *8*, 704.

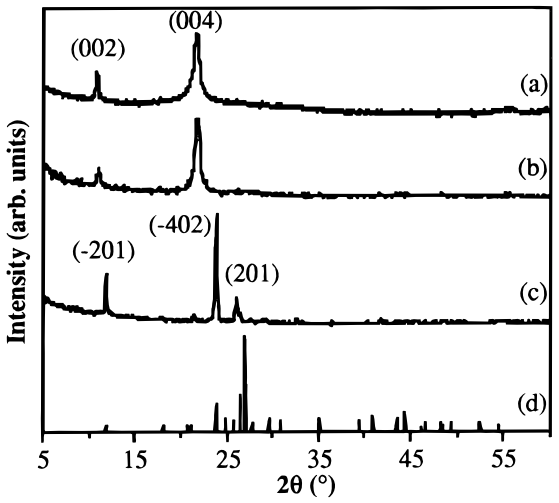

Figure 13. Thin-film X-ray diffraction results for films grown by low-pressure CVD from (a) $[(Me_3C)Ga(\mu_3\text{-}Te)]_4$ at 285 °C, (b) $[(EtMe_2C)Ga(\mu_3\text{-}Te)]_4$ at 310 °C, (c) sample (b) annealed at 500 °C for 17 h with monoclinic (*hkl*) labels, and (d) JCPDS pattern for m-GaTe.

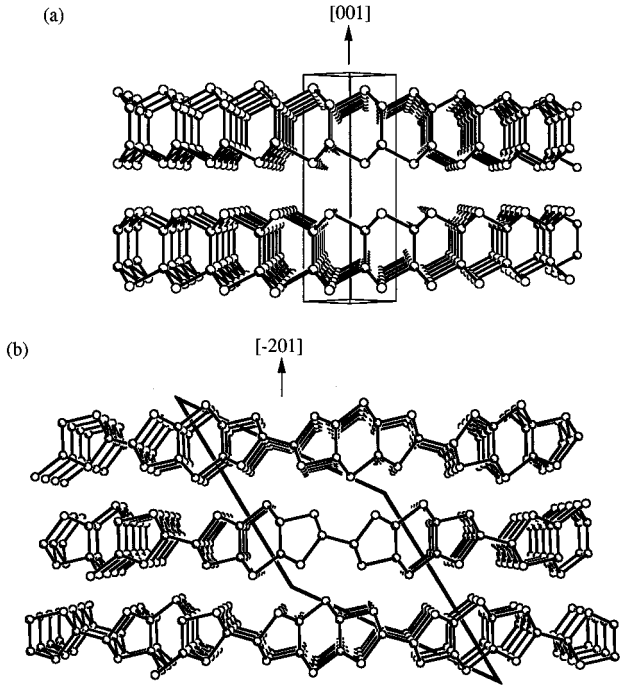

Figure 14. Structural models of the (a) hexagonal ($P6_3/mmc$) phase of GaSe and (b) monoclinic phase ($C2/m$) of GaTe. Gallium atoms are shown shaded.

of every third Ga−Ga moiety in the structure that occurs on going from h-GaTe to m-GaTe (see Scheme 1) does so with little gross lattice reorganization and consequently the overall layer orientation is retained.

It is important at this point to address the large discrepancy between our hexagonal GaTe lattice parameter and that of Semiletov and Vlasov ($\Delta c = 0.58$ Å).[31] First it should be noted that electron diffraction parameters on polycrystalline materials have appreciable error due to uncertainties in measuring rings and Semiletov's pattern consisted of broad textured rings. In contrast, our X-ray results were corrected using a silicon powder external standard. A structural model of h-GaTe using Ga−Ga bond lengths and Ga−Te angles derived from the h-GaSe structure, along with Ga−Te covalent bond lengths yields lattice parameters of $a =$ 4.0 Å and $c = 16.3$ Å. This c axis length is consistent with our value derived from thin-film XRD ($c = 16.38$ Å). It is unlikely that Semiletov's films are larger due to a different stacking sequence since the c parameter must still be a whole number multiple of ca. 8 Å, the size of a Te−Ga−Ga−Te double layer.

Scheme 1. Structural Relationship between h-GaTe and m-GaTe[a]

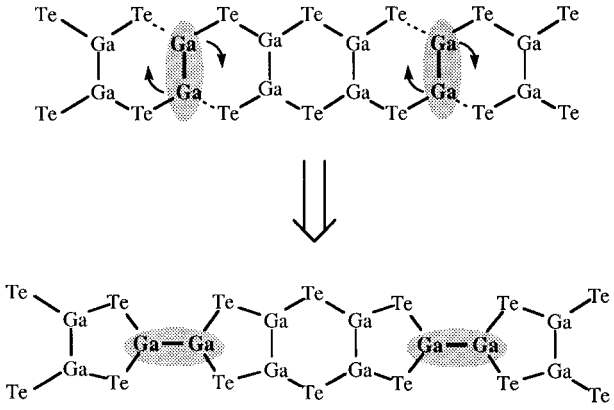

[a] Arrows Indicate the Formal Rotation of the Highlighted Ga−Ga Moieties that Occurs during the Rearrangement.

Cross-sectional TEM of a h-GaTe film shows a less well-defined particle morphology than in GaSe and only weak electron diffraction could be obtained (Figure 15). The layered appearance of the film seen in Figure 15a may be due to variations in precursor delivery (sublimation rate) as the deposition progressed. The particle size is on the order of 5 nm (smaller than in MOCVD grown h-GaSe) and larger amorphous regions than observed in the h-GaSe films may be present. Using the few diffraction spots available, approximate lattice parameters of $a = 4.1$ Å and $c = 16.0$ Å are obtained. The c-axis is consistent within experimental error of the value derived from XRD data and the a-axis is consistent with a structural model described above. A summary of the XRD and TEM diffraction results is given in Table 3.

The stoichiometric m-GaTe phase is a moderate bandgap semiconductor with E_g values of 1.7 eV. Films of h-GaTe grown on fused quartz substrates from the cubane precursors show absorption cutoffs (Figure 8b) yielding optical bandgaps in the range 1.75−1.9 eV, suggesting that the structural differences between h-GaTe and m-GaTe is insufficient to greatly affect the electronic properties. In this regard it is worth noting that the E_g values for h-GaSe (2.0 eV) and cubic Ga_2Se_3 (2.1 eV, defect ZnS structure) are quite similar, while their structures and compositions are very different.

The chemical state and local bonding environment of h-GaTe (and h-GaSe) films were examined by X-ray photoelectron spectroscopy (XPS). The films were cleaned by argon ion sputtering and the resulting peak maxima are reported in Table 6. The binding energies for our h-GaE films are in reasonable agreement within error (±0.5 eV) of the literature values for similar compounds.[32]

Relationship between Precursor Core Cleavage and Deposited Phase. Table 7 summarizes the gal-

(32) Wagner, C. D. *NIST Technical note 1289*, October 1991, National Institute of Standards and Technology.

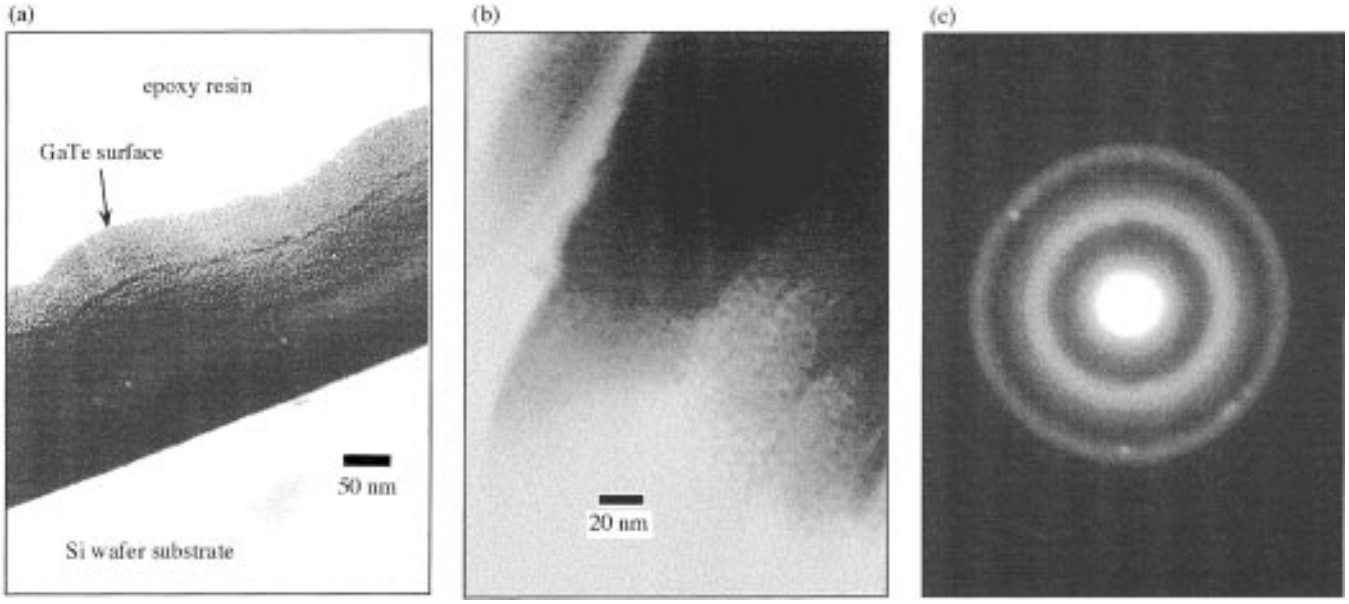

Figure 15. TEM cross-sectional results for a h-GaTe film grown from $[(Et_2MeC)Ga(\mu_3\text{-}Te)]_4$ at 285 °C (a and b) bright field images and (c) their corresponding electron diffraction pattern.

Table 6. XPS Results for Hexagonal GaSe and GaTe Films

compound	Ga 2p (eV)	Se 3d (eV)	Te 3d (eV)
element	18.7	55.1	573.0
Ga_2E_3[b]	19.7	54.6	572.4
h-GaSe	20.1	54.8	n/a
h-GaTe	20.5	n/a	573.0

[a] Referenced to C(1s) at 284.5 eV. [b] Ga and Se values from Ga_2Se_3 and Te from Ga_2Te_3.

Table 7. Summary of the Gallium Chalcogenide Phases Deposited by MOCVD from the Cubane Single-Source Precursors, $[(R)Ga(\mu_3\text{-}E)]_4$, in Comparison to the Thermodynamically Favored Binary Phases

precursor[a]	deposited phase	thermodynamic phase[b]
$[(R)Ga(\mu_3\text{-}S)]_4$	cubic GaS	hexagonal GaS (30,0576)
$[(R)Ga(\mu_3\text{-}Se)]_4$	hexagonal GaSe[c]	hexagonal GaSe[c](37,0931)
$[(R)Ga(\mu_3\text{-}Te)]_4$	hexagonal GaTe[c]	monoclinic GaTe (33,0571)

[a] R = CMe_3, $CEtMe_2$, CEt_2Me. [b] JCPDS file number given in parentheses. [c] Hexagonal-GaS type structure.

lium chalcogenide phases deposited by MOCVD from the cubane single-source precursors, $[(R)Ga(\mu_3\text{-}E)]_4$, in comparison to the thermodynamically favored binary phases. As discussed above, use of $[(R)Ga(\mu_3\text{-}E)]_4$ (E = Se, Te) results in the growth of the hexagonal GaE (h-GaE). In contrast their sulfide analogues allow for the growth of metastable cubic-GaS. Although h-GaSe is the thermodynamically stable binary phase, h-GaTe is a metastable phase. These observations prompt the following questions: First, given that the precursors have the same Ga_4E_4 core structure, why does the sulfide grow as a cubic phase but the selenide and telluride grow as hexagonal phases? Second, why does the selenide grow as the thermodynamically expected hexagonal phase, but the telluride form a *metastable* hexagonal phase?

The similarity of the structure for GaSe and GaTe films suggests that their cubane precursors undergo decomposition via a similar reaction pathway, which is distinct from that of the sulfide precursor. We have previously proposed that the growth of cubic-GaS from $[(Me_3C)Ga(\mu_3\text{-}S)]_4$ is as a consequence of the retention of the "Ga_4S_4" cubane core during deposition.[10,11] This proposal was supported by vapor-phase UV-laser photolysis/time-of-flight mass spectrometry studies[12] which showed that $[(Me_3C)Ga(\mu_3\text{-}S)]_4$ decomposes via consecutive loss of the organic substituents without core cleavage. The antithesis to this observation is that under photochemical-assisted MOCVD conditions the thermodynamically stable hexagonal GaS is observed as a consequence of the photochemical cleavage of the Ga_4S_4 core of the $[(Me_3C)Ga(\mu_3\text{-}S)]_4$ precursor.[33] It is reasonable, therefore, to suggest that the formation of hexagonal GaSe and GaTe is as a consequence of the cleavage of the appropriate Ga_4E_4 core during MOCVD. However, indiscriminate cleavage of the precursor's core would result in the formation of the thermodynamically stable stoichiometric chalcogenides Ga_2E_3, in a manner similar to that observed for the use of the $[(\eta^5\text{-}C_5Me_5)Ga(\mu_3\text{-}E)]_4$ cubanes.[34] Thus, we conclude that the formation of hexagonal GaSe and GaTe must involve the "controlled" cleavage of the appropriate Ga_4E_4 core.

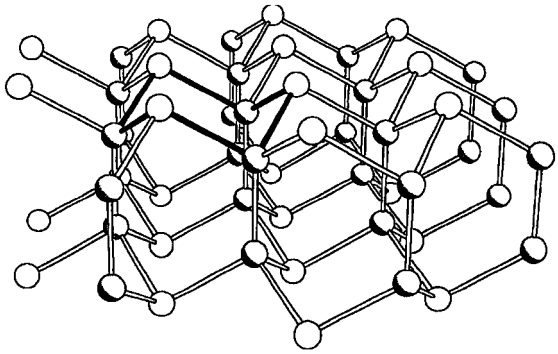

Figure 16. Structure of hexagonal-GaSe. The solid bonds represent the smallest molecular fragment. Gallium atoms are shown shaded.

The structure of hexagonal GaE is shown in Figure 16, with the smallest molecular fragment, a "Ga_3E_3" trimer, highlighted by the bold bonds. In order for highly crystalline GaSe to grow at 350 °C, the Ga_4E_4

(33) Pernot P.; Barron, A. R. *Chem. Vap. Deposition* **1995**, *1*, 75.
(34) Shulz, S.; Gillan, E. G.; Rogers, L. M.; Rogers, R.; Barron, A. R. *Organometallics* **1996**, *15*, 4880.

Scheme 2. Mass Spectral Fragmentation Pattern for $[(R)Ga(\mu_3\text{-}E)]_4$, E = Se, Te and R = CMe_3, $CEtMe_2$, CEt_2Me

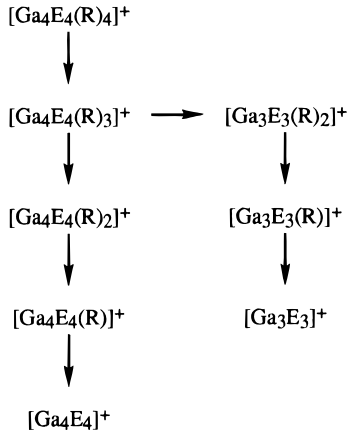

core of $[(R)Ga(\mu_3\text{-}E)]_4$ would be required to undergo significant cleavage. Mass spectral analysis of $[(R)Ga(\mu_3\text{-}Se)]_4$ and $[(R)Ga(\mu_3\text{-}Te)]_4$ (Scheme 2) show prominent $[Ga_3E_3(R)_2]^+$ fragments.[20] Such fragments are not ordinarily observed for $[(R)Ga(\mu_3\text{-}S)]_4$.[12] This is consistent with the decrease in thermochemical bond energies between gallium and the chalcogen down the period, i.e., Ga−S (318 kJ.mol^{-1}), Ga−Se (274 kJ.mol^{-1}), and Ga−Te (251 kJ.mol^{-1}),[35] which in turn relates well to the decrease in deposition temperatures, i.e., GaS (400 °C), GaSe (350 °C), and GaTe (300 °C), despite the near identical Ga−alkyl bond strengths (estimated 235 kJ mol^{-1}) expected in each compound. Thus, we propose that whereas $[(R)Ga(\mu_3\text{-}S)]_4$ decomposes via consecutive Ga−R bond cleavage, $[(R)Ga(\mu_3\text{-}Se)]_4$ and $[(R)Ga(\mu_3\text{-}Te)]_4$ decomposition involves loss of "(R)GaE" (e.g., eq 1),

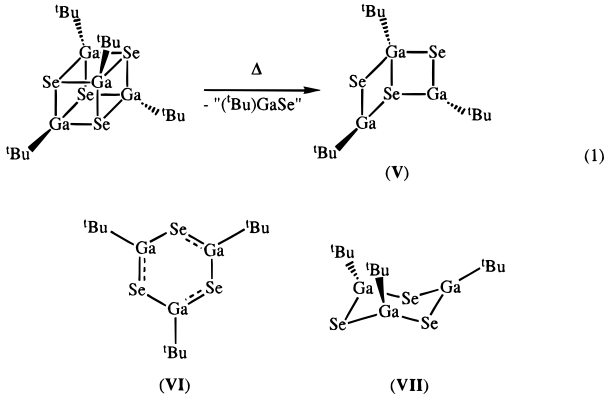

(1)

yielding the "$(R)_3Ga_3E_3$" fragment.[36] The "$(R)_3Ga_3E_3$" moiety (**V**) is isoelectronic with Dewar benzene and upon surface adsorption could rearrange to a Kekulé (**VI**) or cyclohexane (**VII**) form, which are clearly related to the chair Ga_3E_3 conformation fragment present in hexagonal GaE (cf. Figure 16).[37] The similarity of the films

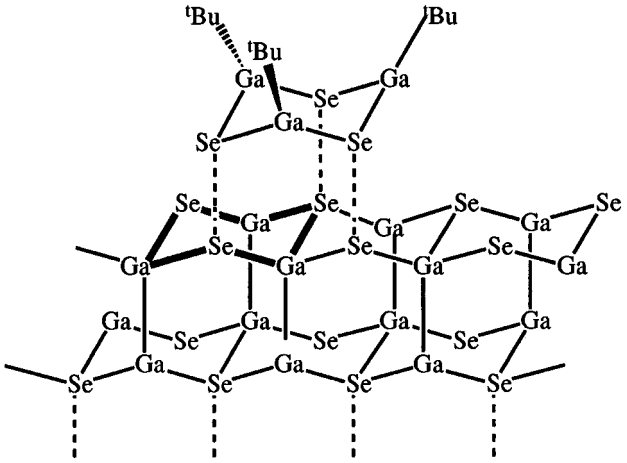

Figure 17. Schematic representation of the condensation of trimeric Ga_3Se_3 fragments to build up the hexagonal GaSe phase.

for GaSe and GaTe suggest that comparable decomposition/growth mechanisms are present.

While the hexagonal GaE phases may be considered to consist of fused six-membered Ga_3E_3 rings in a chair conformation, the monoclinic-GaTe phase consists of fused five- and six-membered cycles (Figure 14b and Scheme 1). While the hexagonal form may be built up from "$(R)_3Ga_3E_3$" moieties, additional ring rupture or rearrangement must occur for the monoclinic form to be deposited. Thus, we propose that the growth of metastable hexagonal GaTe is as a consequence of the partial "controlled" decomposition of the cubane core.

We have previously reported that polycrystalline films of the thermodynamically stable hexagonal phase of gallium sulfide (h-GaS) may be grown from the dimeric precursor, $[(Me_3C)_2Ga(\mu\text{-}SCMe_3)]_2$, under thermal MOCVD conditions,[10] or from $[(Me_3C)Ga(\mu_3\text{-}S)]_4$ by PA-MOCVD.[33] In neither case do the films show any preferred crystal orientation by X-ray or electron diffraction measurements. This is unlike the GaSe and GaTe films discussed herein, which show a high preference for *c*-axis growth irrespective of substrate; see Figures 3 and 13.[38] It is interesting to postulate as to the reason for this difference. The growth of highly oriented GaSe and GaTe irrespective of substrate may be rationalized as being self-consistent with the decomposition pathway discussed above. For example, if decomposition of $[(R)Ga(\mu_3\text{-}E)]_4$ in the vapor phase results in the formation of "$(R)_3Ga_3E_3$" fragments, these fragments may condense to form particles in the vapor phase and/or decompose on the surface to "knit" together particles or islands on the surface. Since upon adsorption on the growth surface, the "$(R)_3Ga_3E_3$" fragment (or larger agglomerates) would align preferentially parallel to the growth surface and aided by van der Waals forces, they would create a *c*-axis perpendicular to the growth surface. As Figure 17 shows, the hexagonal GaE phase may be constructed solely by condensation of these trimeric species. Such a mechanism may explain the formation of Me_3CCMe_3 and the "reduction" of the gallium from Ga^{3+} in the precursor to Ga^{2+} in the deposited films.[39] If the surface reaction

(35) (a) *Handbook of Chemistry and Physics*, 66th ed.; Weast, R. C., Ed.; CRC Press: Boca Raton, FL, 1985. (b) *Lange's Handbook of Chemistry*, 14th ed.; Dean, J. A., Ed.; McGraw-Hill, Inc.: New York, 1992. (c) Kubaschewski, O.; Alcock, C. B.; Spencer, P. J. *Materials Thermochemistry*, 6th ed.; Pergamon Press: New York, 1993.

(36) We have previously observed that the cleavage of the gallium cubane compounds often occurs with formation of Ga_3E_3 trimers, see: Harlan, C. J.; Barron, A. R. *J. Cluster Chem.* **1996**, *7*, 455.

(37) Power, M. B.; Ziller, J. W.; Barron, A. R. *Organometallics* **1992**, *11*, 2783.

(38) There have been some reports of *c*-axis orientation in physical vapor deposition grown films of GaSe, see: Yudasaka, M.; Nakanishi, K. *Thin Solid Films* **1988**, *145*, 152.

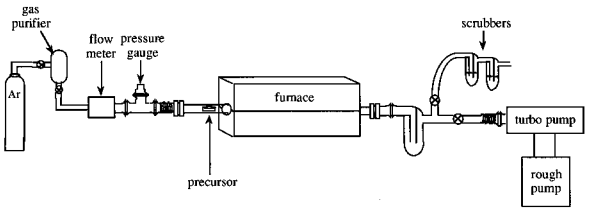

Figure 18. Schematic of experimental system for both atmospheric and low-pressure MOCVD studies using the [(R)-Ga(μ_3-E)]$_4$ cubane precursors.

of the "$(Me_3C)_3Ga_3E_3$" fragments, in which the gallium is formally Ga^{3+}, occurred with reductive elimination of Me_3CCMe_3, then the resulting films would contain Ga−Ga units, i.e., Ga^{2+}. UHV studies on the selenium cubanes are in progress to more accurately determine their gas-phase thermal stability.

Experimental Section

The synthesis and characterization of the cubanes, [(R)Ga-(μ_3-E)]$_4$ (R = CMe_3, $CEtMe_2$, and CEt_2Me; E = Se, Te), used in this study have been described previously.[18,19,20,37,40,41] All precursors were purified by either vacuum sublimation or crystallization prior to use. The thermal stability and volatility characteristics of the precursors were determined by thermogravimetric and differential thermal analysis using a Seiko 200 TG/DTA with heating rates of 5 °C min^{-1} up to 400 °C under either a 200 mL min^{-1} Ar gas flow or a 0.2 Torr dynamic vacuum (Welch DuoSeal pump).

Chemical Vapor Deposition. The deposition of gallium selenide and telluride films was performed using the horizontal flow CVD system shown in Figure 18. This system was designed to allow deposition under variable atmospheric flow or dynamic vacuum conditions. In a typical CVD run, 30−60 mg of the precursor was placed in a small glass boat near the entrance to the furnace. The substrates were loaded into the Pyrex reactor tube and positioned in the center of the furnace, and deposition temperatures and flows were adjusted such that film growth was centered on or near the substrates. Silicon (100) and GaAs (100) substrates were cleaned with 10% HF in ethanol and rinsed with deionized water, while fused quartz substrates were rinsed with acetone prior to use. The entire system was evacuated to a base pressure of 1×10^{-3} Torr and then flushed with prepurified argon (99.999%). Once the desired gas flow was achieved (50−150 mL min^{-1}) and the furnace was heated to the deposition temperature, then the precursor was heated to its volatilization temperature using heating tape. Temperatures in the range 230−270 °C were generally sufficient to produce a steady precursor vapor. In the case of the tellurium precursors, the depositions were carried out under dynamic vacuum (10^{-1}−10^{-3} Torr) with the precursors heated to between 150 and 190 °C (see Tables 2, 4, and 5).

The volatile byproducts were trapped by passing the exhaust gases through a glass bubbler containing $CDCl_3$ cooled in a dry ice/acetone bath (−60 °C). The cooled solution was injected into a gas chromatograph interfaced to a high-resolution mass spectrometer (MAT-250). Mass analysis was conducted up to 300 amu. After the solution was warmed to room temperature the presence of lower volatility species was checked by electron impact (EI) mass spectrometry.

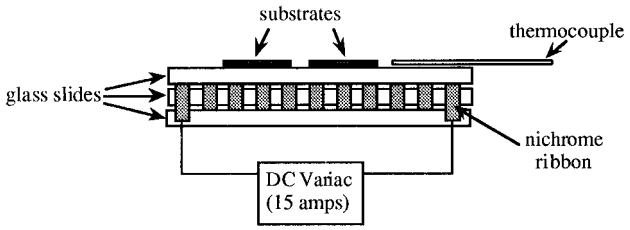

Figure 19. Schematic of substrate heater in warm wall (250 °C) MOCVD flow system.

A series of exploratory experiments were performed in a "warm-walled" MOCVD chamber. The home-built substrate heater (Figure 19) was placed in a Pyrex flow system along with the precursor (ca. 30 mg) in a glass crucible. The system was purged with purified argon then stabilized at 100−150 ccm. The precursor and heater region were then heated to 240 °C to sublime and maintain the precursor in the gas phase. A chromel−alumel thermocouple was in contact with the heater surface near the substrates and temperature was adjusted to 350−370 °C with a variac.

Film Characterization. The GaSe and GaTe films were characterized by thin-film X-ray diffraction using either a Scintag 2000 or Siemens diffractometer. Simulated XRD patterns and structural models were generated from crystallographic data using the SHELXTL software system.[42] Film surface morphology was examined by scanning electron microscopy with a JEOL 6400 or 5300 system. Elemental compositions of films on Si (100) were determined by Rutherford backscattering (RBS), WDS microprobe analysis, Auger electron spectroscopy (AES), and X-ray photoelectron spectroscopy (XPS). RBS measurements were performed using a 3 MeV General Ionx Tandetron and RUMP simulations software. WDS microprobe analysis were obtained on a Cameca SX-50 relative to calibration standards. Auger spectroscopy depth profiling was obtained using a Physical Electronics 660 system. XPS was performed on a Surface Science Instruments Spectrometer (Model SSX-100) with a monochromatized Al Kα source. The spectra were acquired with a 50 eV pass energy and a 1000 μm spot size. All samples were sputtered with 3 keV argon ions prior to data collection to remove adventitious carbon. All spectra were charge referenced independently to graphitic carbon (C_{1s} = 284.5 ± 0.5 eV). The quantitative results reported in the tables are from WDS microprobe data. UV−visible optical absorption measurements were obtained from films deposited on fused quartz using either a Hitachi U4001 or a GBC UV/vis spectrometer. Bandgaps were calculated from extrapolations of the linear portions of transmittance drops. Cross-sectional TEM samples were prepared by thinning an epoxy-encased slice which was ion-milled on a copper grid. Analysis was performed on a JEOL 2010 operating at 200 keV.

Acknowledgment. Financial support for this work is provided by the Office of Naval Research and the National Science Foundation. M. Pearson and T. Marriott (Rice University), E. Shaw (MIT), J. Chervinsky (Harvard University), and D. Callahan (Rice University) are gratefully acknowledged for assistance with microprobe analysis, GC-mass spectrometry, AES, RBS, and TEM measurements, respectively. E.G.G. thanks A. N. MacInnes (TriQuint) for insight and guidance in the early stages of this work.

CM9703886

(39) It has been noted by one of the referees that the presence of a preferred orientation in the films is surprising since they consist of what appear to be near-spherical particles. As spherical crystallites, as indicated from microscopy, it would be expected that a "normal" powder pattern would result. One possible explanation may be that the crystallites are in fact drumlike rather than spherical. However, we have no evidence to preclude an alternative rational for the preferred orientation of the films.

(40) Power M. B.; Barron, A. R. *J. Chem. Soc., Chem. Commun.* **1991**, 1315.

(41) Power, M. B.; Barron, A. R.; Hnyk, D.; McMurdo, G.; Rankin, D. W. H. *Adv. Mater. Optics Electron.* **1995**, *5*, 177.

(42) Nicolet Instrument Corp. *SHELXTL-PLUS Users Manual*, Madison, Wisc., 1988.